In memory of Professor Robert R. Gałązka

Mn Contribution to the Valence Band of $Ga_{0.98}Mn_{0.02}Sb$ — A Photoemission Study

B.J. Kowalski[a,*], R. Nietubyć[b], and J. Sadowski[a,c]

[a] *Institute of Physics, Polish Academy of Sciences, Aleja Lotnikow 32/46, PL-02668 Warsaw, Poland*
[b] *National Centre for Nuclear Research, A. Sołtana 7, 05-400 Otwock, Poland*
[c] *Department of Physics and Electrical Engineering, Linnaeus University, SE-391 82 Kalmar, Sweden*

Doi: 10.12693/APhysPolA.141.175 *e-mail: kowab@ifpan.edu.pl

The contribution of the Mn 3*d* states to the valence band of $Ga_{0.98}Mn_{0.02}Sb$, an important factor determining the properties of this system, including the mechanism responsible for the magnetic characteristics, has been revealed by photoelectron spectroscopy. The resonant photoemission experiment, carried out for photon energies close to the Mn $3d \rightarrow 3p$ excitation, allowed us to identify the spectral feature corresponding to emission from the Mn 3*d* states. The scanning of the valence band along the [100] direction of the Brillouin zone, by the angle-resolved photoemission experiment, showed that these states contributed to a dispersionless structure at the binding energy of 3.6 eV (with respect to the Fermi energy). The revealed shape of the Mn 3*d* contribution is consistent with the supposition that the *p–d* exchange interaction prevails as a mechanism supporting ferromagnetism in $Ga_{1-x}Mn_xSb$.

topics: diluted magnetic semiconductors, resonant photoemission, photoelectron spectroscopy

1. Introduction

A permanent intense interest in technology and properties of $Ga_{1-x}Mn_xAs$ and related solid solutions is another, recent proof of the imperishable topicality of the concept of semimagnetic semiconductors or diluted magnetic semiconductors (DMS). Since the first experimental evidence for the molecular beam epitaxy (MBE) growth of III–V-based DMSs [1], such materials are in the focus of intense investigations, motivated by both curiosity-driven basic research and possible applications. Wide application of III–V-based DMSs in everyday electronics is still hindered by their relatively low Curie temperatures (T_C achieved for $Ga_{1-x}Mn_xAs$ nanostructures equals 200 K [2]), although some concepts of spintronic devices based on them have been demonstrated [3, 4]. Those concepts were based on a combination of ferromagnetic characteristics and electronic properties of semiconductors manifesting themselves in III–V-based DMSs. Therefore, physical mechanisms leading to the ferromagnetic ordering of local moments of Mn atoms are among the most important issues still discussed in the context of the considered materials. The double-exchange and *p–d* exchange interactions are widely considered as two extreme mechanisms leading to the ferromagnetic order [5, 6]. According to the results of theoretical calculations, they dominate in $Ga_{1-x}Mn_xN$ and $Ga_{1-x}Mn_xSb$, respectively. In $Ga_{1-x}Mn_xP$ and $Ga_{1-x}Mn_xAs$, both mechanisms coexist. The debate on the factors determining ferromagnetism in III–V DMSs and on the ways to increase their T_C is still not over [7, 8].

The theoretical conclusions were confronted with the results of suitable experiments, specifically for $Ga_{1-x}Mn_xAs$, a prototype ferromagnetic DMS. In particular, various techniques of photoelectron spectroscopy were used to reveal the Mn 3*d*-derived contribution to the electronic band structure of $Ga_{1-x}Mn_xAs$. Hard X-ray photoemission spectroscopy was applied to find the difference between the band structures of GaAs and $Ga_{1-x}Mn_xAs$, to reveal Mn-induced states above the GaAs valence band maximum together with changes in the whole valence band, and to conclude that ferromagnetism in $Ga_{1-x}Mn_xAs$ appears due to both double exchange and *p–d* exchange interactions [9]. A conclusion that the hole transport in an Mn-induced impurity band stabilizes ferromagnetism in $Ga_{1-x}Mn_xAs$ has been derived from soft X-ray angle-resolved photoemission experiments [10]. A precise low-temperature angle-resolved photoemission study enabled accurate determination of the Fermi level with respect to the

top of the valence band of $Ga_{1-x}Mn_xAs$ [11]. The obtained value for this parameter supported the p–d Zener model of ferromagnetism. The Coulomb gap at E_F was also detected and ascribed to disorder-induced carrier correlations. Subsequent very precise angle-resolved photoemission experiments [12] proved that the band structure of the host crystal was strongly modified by the presence of Mn in a wide energy range. The observations confirmed the location of the main Mn $3d$ peak at about 3 eV [13, 14]. An important finding was revealing a highly dispersive band above the valence band maximum. The band was induced by Mn, i.e, appeared because Mn impurities caused such a change in the host valence band states. This finding allowed for reconciling the p–d Zener model of ferromagnetism in $Ga_{1-x}Mn_xAs$ with previous results of spectroscopic studies. The Bragg-reflection standing-wave hard X-ray angle-resolved photoemission spectroscopy was applied to compare the band structure of GaAs and $Ga_{1-x}Mn_xAs$, to confirm substitutional doping with Mn, and to reveal the influence of Mn throughout the electronic band structure [15].

$Ga_{1-x}Mn_xSb$ exhibits ferromagnetic properties at relatively low temperatures (T_C = 25 K [16]) and it has been investigated much less than $Ga_{1-x}Mn_xAs$ but it still attracts interest due to the opportunity to study the interactions of magnetic ions with charge carriers in a host with anions chemically different than in arsenides or due to the band structure of $Ga_{1-x}Mn_xSb$ particularly suitable for making a novel device (a ferromagnetic resonant interband tunneling diode [17]). Our photoemission study of the $Ga_{1-x}Mn_xSb$ band structure is motivated by the suggestion, based on theoretical studies, that the p–d exchange interactions determine ferromagnetism in this system [18, 19], and therefore we should be able to observe band structure modifications related to this mechanism. Therefore, we used resonant photoemission and angle-resolved photoemission methods to reveal the Mn $3d$-derived contribution against a background of the host band structure.

One of the most important aspects of any photoemission experiment is the preparation of the sample surface. As III–V DMSs exist as epitaxial layers, atomically clean and ordered surfaces cannot be made by cleavage. Any post-growth attempt to clean the surface by sputtering or to remove capping by annealing would change the properties of the sample. Therefore, some of the reported experiments were carried out by bulk-sensitive photoemission techniques [9, 10, 15], the others [11–14] were carried out for samples transferred under UHV conditions directly from the MBE chamber to the photoemission spectrometer. The advantages and disadvantages of those techniques were discussed in detail in [12]. As the latter method undoubtedly gives clean and intact surfaces, we follow the same idea in the reported experiments.

2. Experimental details

The $Ga_{1-x}Mn_xSb$ layers with Mn contents of 2% were grown on GaSb (100) substrates by molecular beam epitaxy at a low substrate temperature of about 230°C. The growth processes were carried out in a KRYOVAK III–V MBE system equipped with six individually shuttered effusion cells enabling epitaxy of a wide range of III–V compounds. The MBE chamber was interlocked with a photoelectron spectrometer of the beamline 41 in the MAX-lab synchrotron radiation laboratory of Lund University (Sweden). The MBE growth was monitored *in situ* by reflection high energy electron diffraction (RHEED). The two-dimensional diffraction patterns (streaks) and distinct RHEED oscillations were observed throughout the growth of the $Ga_{1-x}Mn_xSb$ layers up to their final thicknesses (50 to 300 Å depending on the sample). No signs of secondary phases (segregated MnSb nanocrystals [20]) were detected on RHEED images after the growth. The (100) surfaces of the layers exhibited the low energy electron diffraction (LEED) patterns corresponding to the asymmetric (1×3) reconstruction. The absence of MnSb precipitates in the investigated samples was also confirmed by a comparative *ex situ* study (including the samples containing the precipitates [20]) by scanning electron microscopy.

After the growth, the $Ga_{0.98}Mn_{0.02}Sb$ samples were transferred under UHV conditions directly to the photoelectron spectrometer. The photoemission experiments were carried out at the beamline 41 at MAX-lab. The synchrotron radiation beam from a bending magnet was monochromatized in a toroidal grating monochromator (TGM). The angular and energy distribution of photoelectrons was analyzed with an electrostatic spherical sector analyzer. The overall energy resolution was kept around 150 meV, and the angular resolution was about 2°. The origin of the binding energy scale was set at the Fermi level (determined for a reference metal sample). The angle between the incoming photon beam and the normal to the surface was kept at 45°. The spectra were normalized to the monochromator output and photon flux variations.

The sets of photoemission spectra were collected in the normal emission mode for the photon energy ranges from 30 to 60 eV (in order to observe the Mn $3p \rightarrow 3d$ resonance) and from 50 to 106 eV (to scan the band structure along the [100] direction).

3. Results and discussion

Figure 1a shows a set of photoemission spectra acquired in the normal emission mode for $Ga_{0.98}Mn_{0.02}Sb$ (001) for the photon energy range of 37–60 eV, covering the Mn $3p \rightarrow 3d$ intra-ion transition [21]. The analysis of intensities of the features revealed in these spectra enabled us to use the

resonant photoemission method to reveal the Mn $3d$ contribution to the emission from the valence band of the investigated system.

In a resonant photoemission experiment, the radiation energy is tuned to intra-ion resonant electron excitation, like $3p \rightarrow 3d$ for transition metal atoms, and the relaxation of the excited ions leads to the emission of electrons in a process

$$\mathrm{Mn}\,3p^6 3d^5 + h\nu \rightarrow \left[\mathrm{Mn}\,3p^5 3d^6\right]^* \rightarrow \mathrm{Mn}\,3p^6 3d^4 + \mathrm{e}^-, \tag{1}$$

where $*$ — excited state.

Quantum interference between the process involving intra-ion excitation to discrete states and the regular photoemission to continuum states with free electrons

$$\mathrm{Mn}\,3p^6 3d^5 + h\nu \rightarrow \mathrm{Mn}\,3p^6 3d^4 + \mathrm{e}^- \tag{2}$$

leads to a Fano-type resonance [22]. It manifests itself in the enhancement of Mn $3d$-related emission for photon energies close to the Mn $3p \rightarrow 3d$ transition. In particular, the intensity of the feature at the binding energy of 3.6 eV, marked with a broken line in Fig. 1a, strongly depends on the photon energy. This dependence is shown in Fig. 1b (dots) together with the Fano resonance profile (full line) described by

$$I(\omega) = C\,\frac{(\varepsilon - q)^2}{\varepsilon^2 + 1}, \tag{3}$$

where

$$\varepsilon = \frac{h\nu - h\nu_0}{\Gamma}. \tag{4}$$

The above formula (3) fits the experimental results for $h\nu_0 = 50.2$ eV, $\Gamma = 2.8$ eV, $q = 1.1$, with C as a constant. The photon energy of 50.2 eV corresponds very well to the Mn $3p \rightarrow 3d$ resonance [21].

A comparison of the spectra acquired at the resonance and anti-resonance photon energies (indicated with arrows in Fig. 1b) enabled us to reveal the Mn $3d$-related contribution to the photoemission (see Fig. 1c). These spectra, for 47 and 52 eV (drawn in blue and red, respectively, as shown in Fig. 1c), are normalized with respect to the maximum at 1.6 eV, corresponding to the top valence band of the system. The difference curve ($\Delta I(E) = I_{52\,\mathrm{eV}}(E) - I_{47\,\mathrm{eV}}(E)$) (drawn in green) is a measure of the Mn $3d$ contribution to the emission from the valence band of $Ga_{0.98}Mn_{0.02}Sb$. It has a strong maximum corresponding to the feature manifesting itself in the spectra at the binding energy of 3.6 eV and a "satellite" extending down to about 10 eV.

A comparative theoretical study of the electronic structure of III–V DMSs, reported in [5], showed that the evolution of the electronic band structure from $Ga_{1-x}Mn_xN$ through $Ga_{1-x}Mn_xP$, $Ga_{1-x}Mn_xAs$ to $Ga_{1-x}Mn_xSb$ is consistent with the relative energy positions of the Mn $3d$ states and anion p states and results in a shift of the Mn $3d$ contribution from an impurity band in $Ga_{1-x}Mn_xN$ to a structure deep in the valence band in $Ga_{1-x}Mn_xSb$. In $Ga_{1-x}Mn_xP$ and $Ga_{1-x}Mn_xAs$

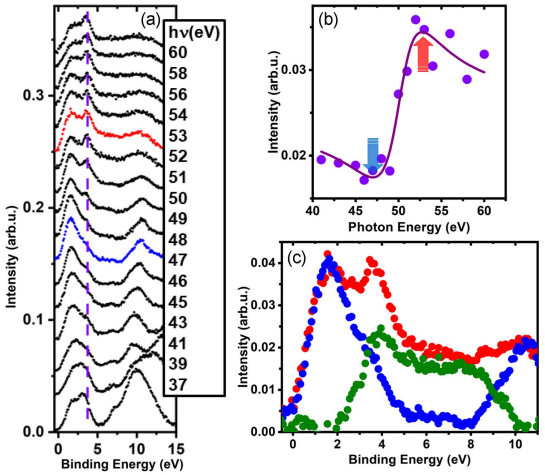

Fig. 1. (a) A set of photoemission spectra acquired in the normal emission mode for $Ga_{0.98}Mn_{0.02}Sb$ (001) for the photon energy range covering the Mn $3p \rightarrow 3d$ resonance. (b) The intensity of the spectral feature at 3.6 eV (marked with a broken line in (a)) as a function of photon energy fit with the Fano profile. The arrows indicate the anti-resonance and resonance energies. (c) The resonance (red), anti-resonance (blue) spectra, and the difference curve ($\Delta I(E) = I_{52\,\mathrm{eV}}(E) - I_{47\,\mathrm{eV}}(E)$) (green) shown as a measure of the Mn $3d$ contribution to the emission from the valence band of $Ga_{0.98}Mn_{0.02}Sb$.

an intermediate situation occurs. As a consequence, it leads to switching the dominating mechanism of ferromagnetism from double exchange to p–d exchange, from $Ga_{1-x}Mn_xN$ to $Ga_{1-x}Mn_xSb$. Therefore, the Mn $3d$ contribution revealed in our resonant photoemission experiment seems to be consistent with that prediction and also with the results of the density of states of $Ga_{1-x}Mn_xSb$ calculations by DFT [23].

Figure 2a shows a set of photoemission spectra acquired in the normal emission mode for $Ga_{0.98}Mn_{0.02}Sb$ (001) for the photon energy increasing from 50 to 106 eV. These spectra were collected as a basis for the construction of the experimental band structure diagram (Fig. 2b) in view of determining the energy position of the Mn $3d$ contribution with respect to the bands of the GaSb matrix. The intensity of the Mn $3d$ contribution was relatively stable for the energies well above the resonance energy, so this feature did not obscure the GaSb-related bands.

The energy positions of features resolved in the spectra were transformed into the experimental band structure diagram (along the Γ–X direction), using the free-electron final state model. Therefore, for the calculation of binding energies of bands and corresponding values for the $\boldsymbol{k}$ vector, the following formula was used

$$k_\perp = \sqrt{\frac{2m}{\hbar^2}\left(E_{\mathrm{kin}} + V_0\right)} - G_\perp. \tag{5}$$

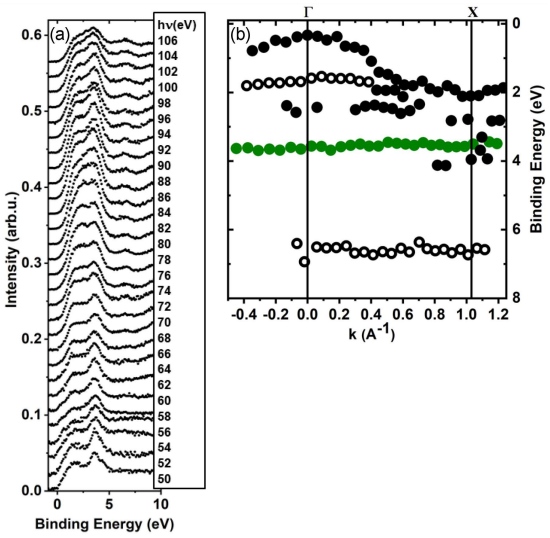

Fig. 2. (a) A set of photoemission spectra acquired in the normal emission mode for $Ga_{0.98}Mn_{0.02}Sb$ (001). (b) The experimental band structure diagram along the Γ–X direction derived from the spectra shown in (a).

The value for the inner potential of the crystal $V_0 = 9.6$ eV was determined by analysis of the curvature of the experimental bands and their symmetry along the $k_\perp$ axis. The diagram shown in Fig. 2b qualitatively corresponds to the results published for GaSb [24]. The black full dots show the top valence band while the heavy and light hole bands are not resolved. Next, the spin–orbit split-off band does not manifest itself clearly in the spectra. As reported in [24], it did not appear close to the Γ and X points. It could be revealed along the Δ direction only close to the centre spot between those high symmetry points, for binding energies of 3–5 eV. For $Ga_{1-x}Mn_xSb$, Mn 3*d* (green full dots) strongly contributes to this part of the diagram, and the corresponding Mn 3*d*-related spectral feature may obscure that of the spin–orbit split-off bulk band. The nondispersive bands (black open dots) correspond well to similar bands revealed for GaSb [24] at the binding energies of 1.7 and 6.6 eV. They were ascribed to indirect transitions or surface-related states. The Mn 3*d* related nondispersive band occurs at 3.6 eV and is discernible across the whole Brillouin zone along the Γ–X direction.

4. Conclusions

Resonance and angle-resolved photoelectron spectroscopies have been used to assess the contribution of the Mn 3*d* states to the valence band of MBE-grown $Ga_{0.98}Mn_{0.02}Sb$, an important factor determining the properties of this system, including the mechanism responsible for the magnetic characteristics. The resonant photoemission experiment was carried out for photon energies close to the Mn $3d \to 3p$ excitation. It allowed us to identify the spectral feature corresponding to the emission from the Mn 3*d* states and to confirm it by revealing the Fano-type profile in its intensity vs photon energy dependence.

The angle-resolved photoemission experiment for $Ga_{0.98}Mn_{0.02}Sb$ (001) in the photon energy range of 50–106 eV was performed to prepare the experimental band structure diagram along the [100] direction in the Brillouin zone. It showed the Mn 3*d*-related nondispersive structure at the binding energy of 3.6 eV (with respect to the Fermi energy). The revealed shape of the Mn 3*d* contribution is consistent with the supposition that the *p*–*d* exchange interaction prevails as a mechanism supporting ferromagnetism in $Ga_{1-x}Mn_xSb$. No Mn 3*d*-related feature has been revealed close to the top of the valence band (a feature potentially confirming the presence of the double exchange mechanism), but this observation should be confirmed by angle-resolved photoemission experiments with higher resolution.

Acknowledgments

This research has received funding from the European Community's Seventh Framework Programme (FP7/2007-2013) under grant agreement no. 226716.

References

[1] H. Munekata, H. Ohno, S. von Molnár, A. Segmuller, L.L. Chang, L. Esaki, *Phys. Rev. Lett.* **63**, 1849 (1989).

[2] L. Chen, X. Yang, F. Yang, J. Zhao, J. Misuraca, P. Xiong, S. von Molnár, *Nano Lett.* **11**, 2584 (2011).

[3] T. Dietl, H. Ono, *Rev. Mod. Phys.* **86**, 187 (2014).

[4] T. Jungwirth, J. Wunderlich, V. Novák et al., *Rev. Mod. Phys.* **86**, 855 (2014).

[5] K. Sato, P.H. Dederichs, H. Katayama-Yoshida, J. Kudrnovský, *J. Phys. Condens. Matter* **16**, S5491 (2004).

[6] K. Sato, L. Bergqvist, J. Kudrnovský et al., *Rev. Mod. Phys.* **82**, 1633 (2010).

[7] L. Gluba, O. Yastrubchak, J.Z. Domagala, R. Jakiela, T. Andrearczyk, J. Żuk, T. Wosinski, J. Sadowski, M. Sawicki, *Phys. Rev. B* **97**, 115201 (2018).

[8] J.-Y. You, B. Gu, S. Maekawa, G. Su, *Phys. Rev. B* **102**, 094432 (2020).

[9] A.X. Gray, J. Minár, S. Ueda et al., *Nature Mater.* **11**, 957 (2012).

[10] M. Kobayashi, I. Muneta, Y. Takeda et al., *Phys. Rev. B* **89**, 205204 (2014).

[11] S. Souma, L. Chen, R. Oszwałdowski, T. Sato, F. Matsukura, T. Dietl, H. Ohno, T. Takahashi, *Sci. Rep.* **6**, 27266 (2016).

[12] J. Kanski, L. Ilver, K. Karlsson, I. Ulfat, M. Leandersson, J. Sadowski, I. Di Marco, *New J. Phys.* **19**, 023006 (2017).

[13] H. Åsklund, L. Ilver, J. Kanski, J. Sadowski, R. Mathieu, *Phys. Rev. B* **66**, 115319 (2002).

[14] I. Di Marco, P. Thunstrom, M.I. Katsnelson, J. Sadowski, K. Karlsson, S. Lebegue, J. Kanski, O. Eriksson, *Nature Commun.* **4**, 2645 (2013).

[15] S. Nemšák, M. Gehlmann, Ch.-T. Kuo et al., *Nature Commun.* **9**, 3306 (2018).

[16] F. Matsukura, E. Abe, H. Ohno, *J. Appl. Phys.* **87**, 6442 (2000).

[17] I. Vurgaftman, J.R. Meyer, *Appl. Phys. Lett.* **82**, 2296 (2003).

[18] T. Dietl, H. Ohno, F. Matsukura, J. Cibert, D. Ferrand, *Science* **287**, 1019 (2000).

[19] Hsiao Wen Chang, S. Akita, F. Matsukura, H. Ohno, *Appl. Phys. Lett.* **103**, 142402 (2013).

[20] K. Lawniczak-Jablonska, A. Wolska, M.T. Klepka et al., *J. Appl. Phys.* **109**, 074308 (2011).

[21] B. Sonntag, P. Zimmermann, *Rep. Prog. Phys.* **55**, 911 (1992).

[22] U. Fano, *Phys. Rev.* **124**, 1866 (1961).

[23] N. Seña, A. Dussan, F. Mesa, E. Castaño, R. González-Hernández, *J. Appl. Phys.* **120**, 051704 (2016).

[24] G.E. Franklin, D.H. Rich, A. Samsavar, E.S. Hirschorn, F.M. Leibsle, T. Miller, T.-C. Chiang, *Phys. Rev. B* **41**, 12619 (1990).